Tracking unstable steady states by large-amplitude low-frequency periodic modulation of a control parameter: Phase-space analysis

A. Kul'minskii,[1,*] R. Vilaseca,[1] and R. Corbalán[2]
[1]*Departament de Física i Enginyeria Nuclear, Universitat Politècnica de Catalunya, Colom 11, E-08222 Terrassa, Spain*
[2]*Departament de Física, Universitat Autònoma de Barcelona, E-08193 Bellaterra, Spain*
(Received 8 July 1999)

Inhibition of chaos in a dissipative nonlinear system that is slowly (nonresonantly) modulated across an instability domain of a fixed-point solution is investigated in detail, considerably extending previous analyses. Comparison is made between the evolution of the modulated system and the evolution of the steady-state solution in phase space as a function of the modulation parameter. It is shown that tracking of the steady-state solution across the instability domain (which can be achieved for a wide domain of modulation frequencies) occurs in a nonintuitive way, as a result of the combination of two factors, which can be present in many nonlinear systems.

PACS number(s): 05.45.−a, 42.60.Mi, 42.60.Fc, 42.65.Sf

I. INTRODUCTION

Much effort has been devoted in the last years to the control of chaotic systems and stabilization of periodic and steady states [1–3], for which different methods have been developed. Essentially, these methods can be classified into two main groups which differ in the type of control signal that is applied to the system. In one of these groups [2] a small-amplitude feedback control signal is applied, at appropriate times, to one of the parameters of the system. In the other group [3], it is a small-amplitude periodic control signal that is applied to a system's parameter. In both cases, it is considered that the small-amplitude control signal does not alter the structure of the system.

A different problem of elimination of chaos arises when a system working on a steady-state regime needs to be periodically modulated, with large modulation amplitude, and this modulation forces the system to penetrate back and forth a domain where the steady-state solution is unstable (Refs. [4,5] and references therein, [6]). If the modulation frequency is much smaller than the natural frequencies of the system, a good reference to study the system's behavior in phase space is the branch of steady-state solutions of the unmodulated system that correspond to the sequence of values of the modulation parameter along one modulation period. In [6] it was shown that for several well-known nonlinear systems and for a wide domain of modulation frequencies (always below the natural frequencies of the system), the system was able to closely follow the steady state's branch across all the unstable domain, inhibiting appearance of chaos. No control signal other than the large-amplitude low-frequency modulation signal was necessary to be applied to the system to achieve tracking of the steady-state solution. This theoretical prediction of Ref. [6] was experimentally demonstrated with a far-infrared ammonia laser [7], and qualitatively similar theoretical predictions [8]—about total or partial inhibition of chaos and reduction of complexity—and corresponding experimental verifications [8] were made for other modulated systems working on periodic orbits instead of steady states.

In Ref. [6], however, there was no detailed analysis of what occurs in the phase space, in the neighborhood of the fixed-point solution, that could allow us to understand how chaos can be inhibited in such a wide domain of modulation frequencies. In this paper we considerable extend the analysis of Ref. [6] by performing such a detailed analysis in the phase space. By studying the linear stability of the branch of steady-state solutions and the relative evolution of the modulated system with respect to this branch, we are able to identify the key features that allow us to understand how steady-state tracking and chaos inhibition occur. As will become evident, they occur in a nonintuitive way.

As in [6], two different cases of modulation involving subcritical and supercritical Hopf bifurcations, respectively, and different types of penetration within the unstable domain, will be considered. Although the efficiency of tracking is larger in the second case to be presented, we start first with a simpler case where the phase-space is only three dimensional (3D) and thus can be more easily represented.

II. LORENZ MODEL

The first case we consider is that of the Lorenz model, because of its simplicity and relevance to fluid and laser dynamics [9]. The equations (expressed in a form convenient to describe a resonant two-level laser), with their three parameters (A, σ, b) and three variables (E, P, D), are explicitly given and defined in [6] [see Eqs. (1) for $\delta=0$ in that reference]. The steady-state nontrivial solution is given by

$$E_s=\pm\sqrt{A-1},\quad P_s=\pm\sqrt{A-1}/A,\quad D_s=1/A, \qquad (1)$$

where A (which represents the pumping rate in the case of a laser) is the parameter that will undergo the slow large-amplitude modulation.

*Permanent address: Institute of Molecular and Atomic Physics, National Academy of Sciences, F. Skaryna Ave. 70, 220072 Minsk, Belarus.

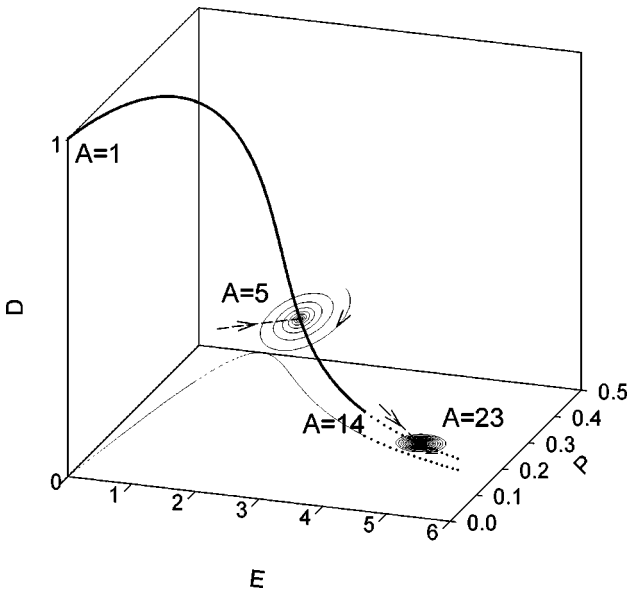

FIG. 1. Thick line: evolution of the steady-state solution of the Lorenz-Haken model in the phase space (E, P, D), when pumping A is varied from 1 to 30. Other parameters are fixed at $\sigma=2$ and $b=0.25$. Continuous (dotted) line indicates stable (unstable) steady state. The subcritical Hopf bifurcation appears at $A=14$. Two spiral lines (one attractive at $A=5$ and one repulsive at $A=23$) show the two-dimensional local manifold at these points, and the dashed lines show the corresponding one-dimensional attractive manifolds. The projection of the steady-state curve on the plane (E, P) is also shown (thin line).

In the absence of modulation, the stability of the steady-state solution (1) is determined by the following three characteristic exponents:

$$\lambda_1 = S + \frac{Q}{S} - \frac{a_1}{3}, \tag{2}$$

$$\lambda_{2,3} = -\frac{S}{2} - \frac{Q}{2S} - \frac{a_1}{3} \pm i\frac{\sqrt{3}}{2}\left(S - \frac{Q}{S}\right),$$

where $S = \sqrt[3]{(R^2 - Q^3)^{1/2}} - R$, $R = \frac{1}{54}(2a_1^3 - 9a_2a_1 + 27a_3)$, $a_1 = b + \sigma + 1$, $a_2 = b(\sigma + A)$, $a_3 = 2\sigma b(A-1)$, and $Q = \frac{1}{9}(a_1^2 - 3a_2)$, with $R^2 - Q^3 > 0$ in the region of parameters here considered. λ_1 is always real and negative, whereas λ_2 and λ_3 can have a negative or positive real part. The change of sign in the real part of $\lambda_{2,3}$ occurs at a subcritical Hopf bifurcation point $A_{HB} = \sigma(b+\sigma+3)/(\sigma-b-1)$. Above this value, the system falls on the well-known Lorenz chaotic attractor (which exists in the domain $A > A_{CH}$, where A_{CH} is smaller than A_{HB}). Figure 1 shows the branch of steady-state solutions (1) that is generated when A is continuously increased from 1 to nearly 30, in a case with $b=0.25$ and $\sigma=2$. In the example considered in the figure the Hopf bifurcation occurs at $A_{HB}=14$. Also shown are two spiral trajectories corresponding to the two-dimensional (2D) focus-type manifold associated with $\lambda_{2,3}$. This 2D manifold is stable for $A < A_{HB}$ and unstable for $A > A_{HB}$. The dashed lines represent the 1D stable manifold associated with λ_1. Figure 2 shows the values of λ_1, λ_2, and λ_3 as a function of A, in the domain $5 \leqslant A \leqslant 23$, which will be considered later. Clearly,

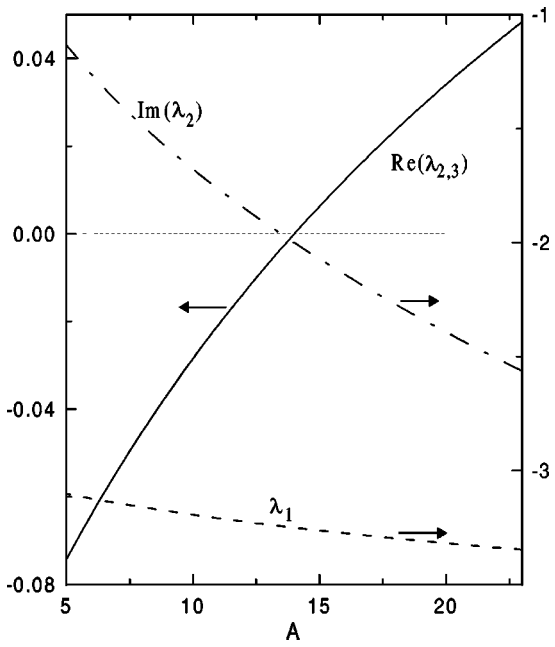

FIG. 2. Variation of the real eigenvalue λ_1 (dashed line) and real (continuous line) and imaginary (dashed-dotted line) parts of the complex-conjugate pair of the eigenvectors $\lambda_{2,3}$ versus pumping A. The arrows indicate the vertical scales associated with each curve. The dotted line depicts the zero level for the curve $\mathrm{Re}(\lambda_{2,3})$. Other parameters as in Fig. 1.

$|\lambda_1| > |\mathrm{Im}\,\lambda_2| > |\mathrm{Re}\,\lambda_{2,3}|$. Finally, Fig. 3 shows, for the same case as Fig. 2, the angle α between the branch of steady states and the 2D local manifold (which is unstable for $A > A_{HB}$ and stable for $A < A_{HB}$), at each point along the branch. As can be seen, this angle (whose precise definition is given in the figure caption) is very small, especially in the unstable region.

We now introduce the modulation in the form $A(t) = A_0 + m\cos(\Omega t + \varphi)$, where the amplitude m can be large and the modulation frequency Ω will be much smaller than the relaxation rates of the system. Since these rates are $O(1)$, this

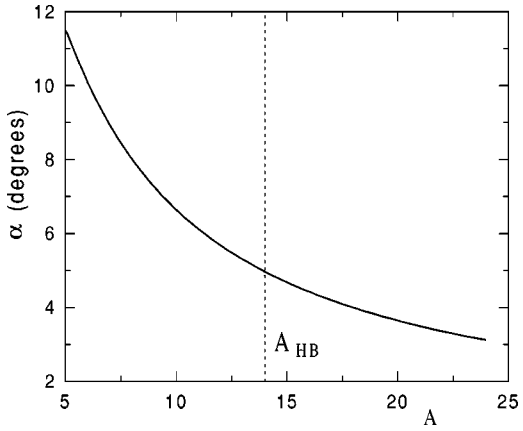

FIG. 3. Dependence of the angle α between the attractive or repulsive local two-dimensional manifold and the curve of steady states (see Fig. 1) on the pumping parameter A. For each value of A, the angle α is obtained by calculating the angle between the tangent to the curve of steady states and the projection of this curve on the local two-dimensional manifold.

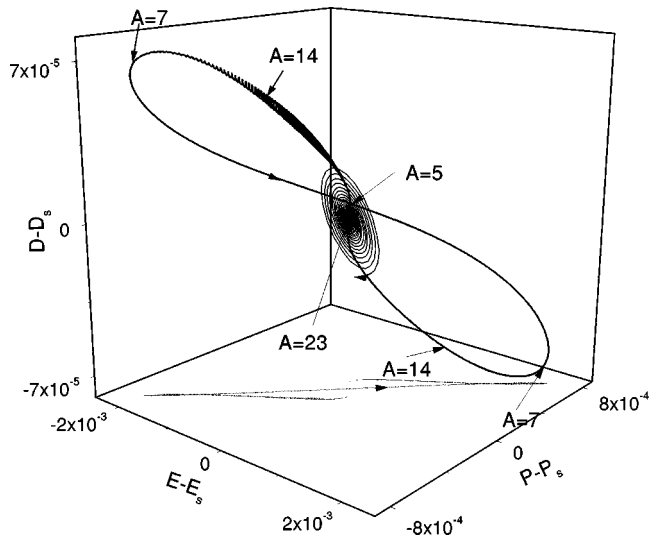

FIG. 4. Trajectory (thick line) of the deviation vector **d** in the phase space (E, P, D), when the modulation range is from $A=5$ to $A=23$ (the projection on the horizontal plane is also included as a thin line), for the case considered in Fig. 1. The spiral line shows the two-dimensional unstable manifold corresponding to $A=23$.

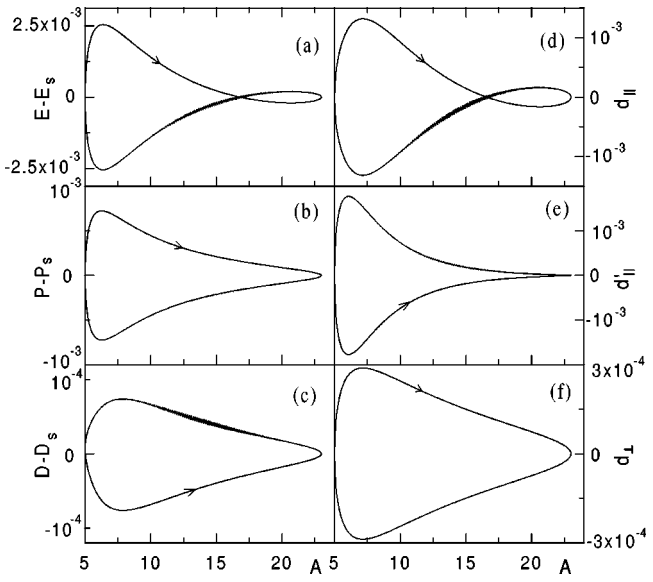

FIG. 5. Left column: the three components of the vector **d** on the axes (E, P, D) are plotted as a function of the instantaneous value of the pumping parameter A. Right column: the same as in the left column, except that now the projections of **d** are on the attractive or repulsive two-dimensional manifold ($d_\parallel$, $d'_\parallel$) (d),(e) and on the attractive one-dimensional manifold ($d_\perp$) (f) versus pumping. Arrows show the direction of the movement starting from the lowest pumping value $A=5$.

means that $\Omega \ll 1$. In [6] it was shown that if A_0 and m are chosen in such a way that the system at each period crosses the bifurcation point A_{HB} back and forth, the system closely tracks the steady-state solution (1) following its periodic movement along the branch depicted in Fig. 1 and never falling into the chaotic attractor. This occurs for any initial conditions and any initial phase φ (the initial conditions only determine the duration of a transient period) and for a wide domain of values of Ω, which covers the range 10^{-3}–10^{-2} and depends also on the values of A_0 and m. As an example of such regular evolution, see Fig. 1 in Ref. [6], which corresponds to the case $A_0=14$, $m=9$, and $\Omega=0.005$.

In order to investigate how this steady-state tracking occurs, Fig. 4 shows the trajectory in phase space of the vector $\mathbf{d}(t)=\mathbf{x}(t)-\mathbf{x}_s(t)$ (thick continuous line), where $\mathbf{x}(t)=(E(t), P(t), D(t))$ is the instantaneous ''position'' of the modulated system and $\mathbf{x}_s(t)=(E_s(t), P_s(t), D_s(t))$ given by expressions (1) with $A\equiv A(t)=A_0+m\cos(\Omega t+\varphi)$ is the instantaneous position of the steady state, which moves along the curve of Fig. 1. We have assumed $A_0=14$, $m=9$, and $\Omega=0.005$, so that $A(t)$ oscillates from 5 to 23: $5\leqslant A(t)\leqslant 23$ (the rest of the parameters are as in Fig. 1). Also depicted, for comparison, is an outward spiral trajectory that corresponds to the 2D unstable manifold for $A=23$; this trajectory is centered at the point (0,0,0). Comparison between Figs. 4 and 1 shows that things occur in a nonintuitive way.

First, there is no inertial delay of the modulated system $\mathbf{x}(t)$ with respect to the unmodulated system $\mathbf{x}_s(t)$; on the contrary, $\mathbf{x}(t)$ ''advances'' $\mathbf{x}_s(t)$ in its movement, i.e., the vector $\mathbf{d}(t)$ points approximately in the same direction as the displacement of $\mathbf{x}_s(t)$, both when A increases and when it decreases.

Second, the spiral component of the $\mathbf{d}(t)$ motion at the frequency $|\mathrm{Im}\lambda_{2,3}|\sim 400\Omega$ (see Fig. 2) is very small (in Fig. 4 it is only noticeable near $A=14$ when A is decreasing). Instead of that, one would have expected a much larger amplitude of the rotation component, with a radius of the order of the distance $|\mathbf{d}(t)|$ to the fixed point, since the displacement of the steady-state point along the branch depicted in Fig. 1 is almost parallel to the 2D manifold defined by the spiral trajectory ($\alpha\lesssim 10°$, Fig. 3) and in addition the system is strongly attractive in the orthogonal direction, Fig. 2.

Third, the modulus of $\mathbf{d}(t)$ in Fig. 4 takes its minimum value not only at $A=5$ (which is normal, since $A=5$ corresponds to the point deepest inside the stable domain, Fig. 1, and where the modulation speed is minimal) but also at $A=23$ (which was unexpected, since it corresponds to the point deepest inside the unstable domain and where the modulation speed is again minimal). In fact, the value of $\mathbf{d}(t)$ at $A=23$ is even smaller than at $A=5$ [$\mathbf{d}(t)=0$ at $A=23$]. Since $\mathrm{Re}(\lambda_{2,3})/\Omega$ varies from ~ -10 [at $A(t)=5$] to $\sim +10$ [at $A(t)=23$], one would have expected the modulus of $\mathbf{d}(t)$ to continuously increase as the system enters the unstable domain $A>14$ and to continuously decrease when the system again enters the stable domain $A<14$.

Several of these features as well as some further details can be more clearly observed in Fig. 5, which shows the parametric dependence of the vector **d** on A along one modulation period. The first column [Figs. 5(a),(b),(c)] shows the components of this vector on the three axes E, P, D considered in Figs. 1 and 4, whereas the second column shows the projections of **d** on the 2D local stable or unstable manifold [Figs. 5(d),(e)] and on the 1D stable manifold [Fig. 5(f)]; we have taken into account that the orientation of these manifolds changes when A varies. As pointed out above, in the neighborhood of the extremal value $A=23$ the modulus of **d** does not monotonically increase, nor does the spiral rotation start to show up. On the contrary, the modulus of **d** takes its smallest value. Because of the exact coincidence between

$\mathbf{x}(t)$ and $\mathbf{x}_s(t)$ at $A=23$, divergence between these two vectors can only occur after crossing that point, i.e., in the interval going from $A=23$ to $A=14$, the point at which the steady state again becomes attractive. Since this interval is small, this explains why tracking of the steady state and inhibition of chaos can be achieved for a wide domain of values of Ω (and of other system parameters). Divergence between $\mathbf{x}(t)$ and $\mathbf{x}_s(t)$ in the interval going from $A=23$ to $A=14$ is manifest in Figs. 4 and 5 not only as an increase of the modulus of $\mathbf{d}$ but also through the appearance of a small-amplitude rotation which is reminiscent of the rotation of trajectories on the 2D unstable manifold. If Ω is progressively reduced (from the value $\Omega=0.005$ considered in Figs. 4 and 5), the amplitude of this rotation component increases and the system eventually falls into chaos, destroying the steady-state tracking process.

Another unexpected feature in Fig. 5 is that the largest separation between $\mathbf{x}(t)$ and $\mathbf{x}_s(t)$ [i.e., the largest $|\mathbf{d}(t)|$] does not occur within the unstable domain but at $A(t)\simeq 6-7$, i.e., quite close to the point $(A=5)$ deepest inside the stable domain; and also that it is in the very close neighborhood of this point, $A=5$ (in which the modulation speed is minimal), that the rate of variation of $|\mathbf{d}(t)|$ with A is maximal.

All these features demonstrate that the effect of modulation on a system, even when this modulation is slow, can significantly modify its dynamics in a way hardly predictable from simplistic models. In fact, large effects of slow parameter sweeping or modulation on the behavior of nonlinear dissipative systems have already been reported in the past [10,11].

III. DETUNED LORENZ-HAKEN LASER

The Lorenz equations can be generalized to describe a two-level laser that can work with detuning between the frequencies of the cavity and the atomic transition [12,9,6]. In this case, the variables E and P become complex: $\tilde{E}(t)=E(t)\exp\{i\varphi(t)\}$ and $\tilde{P}(t)=P(t)\exp\{i\varphi(t)\}$, where $E(t)$ is now a real amplitude, $\varphi(t)$ is the instantaneous field phase (which can be eliminated from the laser equations), and $P(t)\equiv V(t)+iW(t)$ is in general complex. The system now becomes described by four real equations:

$$\dot{E}=-\sigma(E-AV),$$

$$\dot{V}=-V-(1+\sigma)W\delta+W^2\sigma A/E+DE,$$

$$\dot{W}=-W+(1+\sigma)V\delta-V\sigma AW/E, \qquad (3)$$

$$\dot{D}=-b(D-1)-bVE,$$

where δ is a quantity proportional to the cavity detuning. For $\delta=0$, $W=0$ and the previous case is recovered. The nontrivial steady-state solution of this system is now

$$E_s=AV_s=AW_s/\delta=\pm\sqrt{A-1-\delta^2}, \qquad (4)$$

$$D_s=(\delta^2+1)/A.$$

It is well known that for sufficiently large $|\delta|$ this solution is always stable. By decreasing $|\delta|$ a supercritical Hopf bifurcation is found at a certain value $|\delta|=\delta_{HB}$. Further decreasing $|\delta|$ brings about a period-doubling sequence that leads the system into chaos (provided that a value of $A>A_{CH}$ is considered, see Sec. II), whose maximum complexity is reached at $\delta=0$.

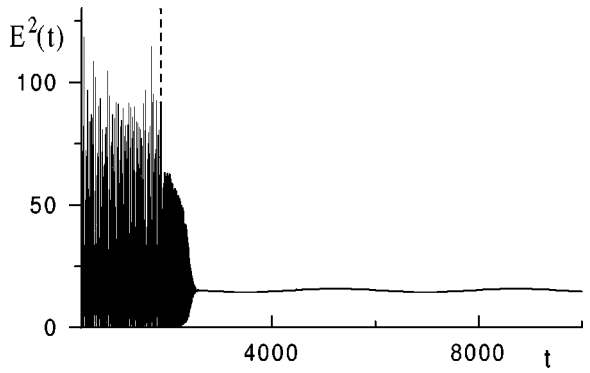

FIG. 6. Laser field intensity $E^2(t)$ as a function of time for $\sigma=2$, $b=0.25$, $A=17$. Detuning modulation with parameters $m=1.2$, $\Omega=0.0009$, and $\delta_0=\varphi=0$ is switched on at the vertical dashed line.

In [6] it was shown that by periodically modulating δ in the form $\delta(t)=\delta_0+m\cos(\Omega t+\varphi)$ the system can cross all the unstable domain (which goes from δ_{HB} to $-\delta_{HB}$) closely tracking the unstable steady state and thus never falling into chaos. Figure 6 shows an example of such behavior in a case where initially the system was in the chaotic attractor. The tracking efficiency was shown to be extremely large, since it could be achieved for values of Ω covering the range 10^{-1}–10^{-4} (and even below for some particular conditions).

In this case, the local unstable manifold of the steady-state solution (4) is again determined by two complex-conjugate eigenvalues, which are denoted by λ_3 and λ_4 in Fig. 7(b), whereas the local stable manifold now is 2D and is described by two eigenvalues λ_1 and λ_2 [Fig. 7(a)], which for small $|\delta|$ are real and for large $|\delta|$ are complex conjugate. Figure 8 is the equivalent to Fig. 2 in the present case: the angle α describes the local angle between the steady-state branch and the 2D unstable manifold in phase space, as a function of the modulation parameter δ, for a case with $\sigma=2.0$, $b=0.25$, and $A=17$, as in Fig. 6. Note from Fig. 8 that now the evolution of the steady-state position in phase space upon parameter modulation is very different from that found in the

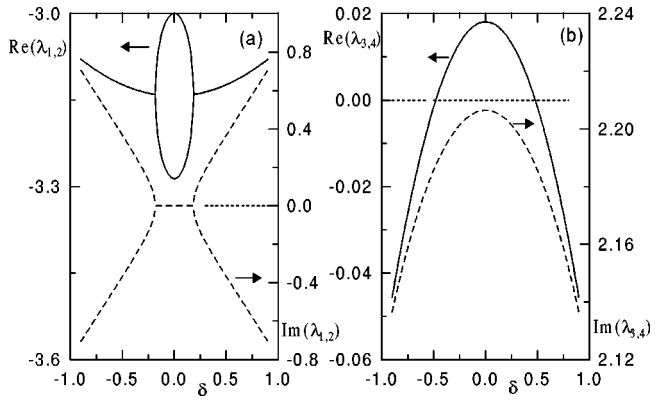

FIG. 7. The same as in Fig. 2 but for the case of detuned laser at fixed pumping $A=17$.

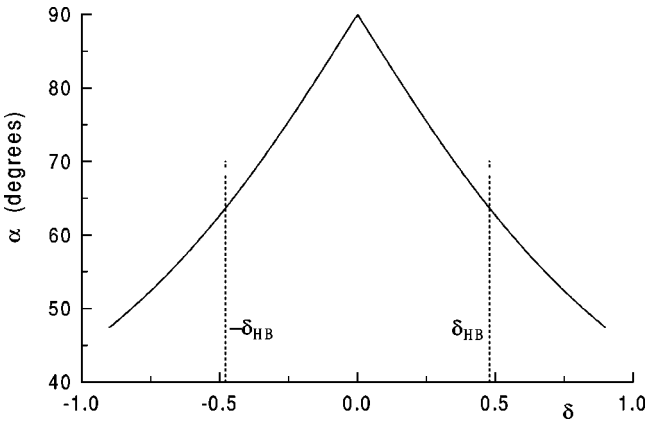

FIG. 8. The same angle as in Fig. 3 but versus detuning δ. Vertical dashed lines show the Hopf bifurcation threshold for symmetrical values of the detuning.

previous case, since it takes place in a direction almost perpendicular to the 2D unstable manifold ($60° < \alpha < 90°$).

To consider the effect of modulation of δ, we choose, for instance, $m=0.9$ and $\Omega=0.0007$. The fact that now $\alpha \sim 90°$ and $\mathrm{Re}(\lambda_{1,2})/\Omega \sim 4\times 10^3$ [which is one order of magnitude larger than $\mathrm{Re}(\lambda_1)/\Omega$ in the case of Sec. II] suggests that, in principle, the instantaneous state of the system will remain, upon parameter modulation, closer to the steady-state point than in the case considered in Sec. II. [Now, however, $\mathrm{Re}(\lambda_{3,4})/\Omega \sim 30$ at the center of the unstable domain ($\delta=0$), which is also several times larger than in the case of Sec. I, but this could be compensated by the fact that in the stable domain this ratio is also larger, in modulus, than before (~ -60 at $|\delta|=0.9$).] Figure 9 shows the parametric dependence on δ of the vector $\mathbf{d}=\mathbf{x}-\mathbf{x}_s$, where $\mathbf{x}=(E, V, W, D)$ is the instantaneous vector describing the modulated system and $\mathbf{x}_s=(E_s, V_s, W_s, D_s)$ is the ''instantaneous'' steady-state solution. Figures 9(a–d) show the projection of $\mathbf{d}$ on the axes E, V, W, and D, respectively [the projections of $\mathbf{d}$ on the unstable manifold are similar to Figs. 9(a) and (b), and the projections on the stable manifold are similar to Fig. 9(d)]. Features similar to those described in Fig. 5, again in contradiction with simplistic expectations, are found.

First, the modulated system state coincides with the steady state just at the center of the unstable domain (i.e., at $\delta=0$). This, as before, is crucial for the efficiency of the tracking process, since it again implies that instability (in the form of a fast rotation component) can only grow in a reduced fraction of the modulation period, after crossing the point $\delta=0$ and before entering the stable domain (in Fig. 9 the rotation component is noticeable between $\delta=0.3$ and 0.7 and between -0.3 and -0.7). Coincidence between $\mathbf{x}$ and $\mathbf{x}_s$ at $\delta=0$, however, occurs only for the components E, V, and D, but it does not occur for the component W [Fig. 9(c)], whose modulus is maximum at $\delta=0$. This feature seems to be directly related to two other features: (i) Analysis of the dependence of the steady-state solution (4) with δ and comparison with Fig. 9 shows that whereas the variables E, V, and D are always ''advanced'' in phase space with respect to the steady-state position [i.e., the point representing the modulated system in the subspace (E, V, D) moves in approximately the same direction as the point representing the steady-state solution and appears in front of it], as in the case considered in Sec. II, the variable W is always ''delayed'' (i.e., it evolves behind the steady-state point). (ii) E_s, V_s, and D_s have a local maximum (case of E_s and V_s) or minimum (case of D_s) at $\delta=0$, whereas W_s has no local maximum within the modulation interval. All this allows us to interpret the coincidence $E=E_s$, $V=V_s$, and $D=D_s$ at $\delta=0$ as a requirement necessary to keep ''advancement'' of these variables E, V, and D with respect to their steady-state values in the whole modulation period (i.e., $E-E_s$, $V-V_s$, and $D-D_s$ must change sign at $\delta=0$). In contrast, for the ''delayed'' variable W the previous condition on the change of sign of $W-W_s$ at $\delta=0$ is not necessary and, in effect, it is not met. Nevertheless, this does not seem to have any influence on the success of the tracking procedure.

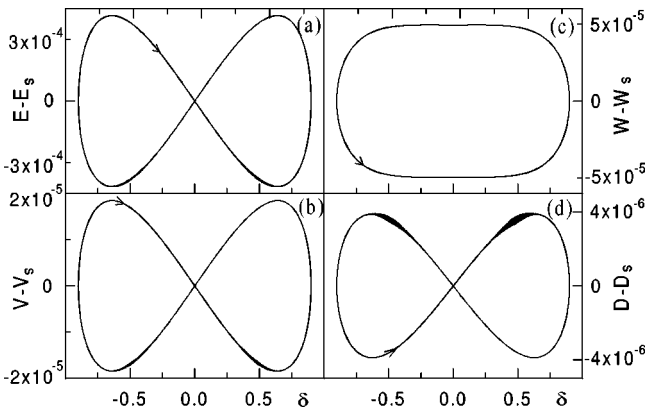

FIG. 9. Dependence of the four components of the vector $\mathbf{d}$ on the detuning δ, for the case considered in Figs. 7 and 8.

Second, the small rotating component that appears after crossing the point $\delta=0$ (from $\delta=0.3$ to 0.7 and from -0.3 to -0.7 in Fig. 9) decreases, as before, with increasing Ω, and increases with decreasing Ω up to the point that eventually can bring the system into chaos.

Third, also as in Fig. 5, the maximum distance between the modulated and unmodulated system solutions is not reached within the unstable domain but near the most stable points $\delta=\pm 1$ (approximately at $\delta=0.7$). It is also worth noting that if Fig. 9 is recalculated for the case $\Omega=0.005$ (to have the same value as in Fig. 5), it is found that the modulus of $\mathbf{d}$ reaches values smaller than those obtained in Fig. 5, a fact that can be attributed to the different value of the angle α in both cases.

Qualitatively similar features are also found in a much more complex model of an optically pumped laser with pump polarization modulation, which are not reported here for the sake of brevity [13].

IV. CONCLUSIONS

In conclusion, in our detailed analysis of the evolution in phase space of a slowly modulated nonlinear system that penetrates or crosses back and forth an unstable domain of the parameter space has allowed us to understand the way in which the system can track, with no control signal, a steady-state solution across the unstable domain. This fact occurs in many systems for a wide domain of modulation frequencies well below the natural evolution frequencies of the system. We have found, in particular, that such efficient tracking oc-

curs because of the presence and combination of the following two factors.

(i) The steady-state fixed point changes the sense of its displacement in phase space at a certain value of the modulation parameter that lies within the unstable domain (it was $A=23$ in the example of Figs. 1–5 and $\delta=0$ in that of Figs. 6–9).

(ii) The modulated system does not follow the displacement of the steady-state point in phase space going ''behind'' that point, but going ''in front of'' it.

Both factors must be met for most of the system's variables (or phase space projections).

Combination of these two factors implies that, necessarily, the distance between the modulated and unmodulated systems in phase space decreases to zero just when the fixed point changes its displacement sense. This leaves only a reduced fraction of the total modulation period available for growing divergence between the modulated and unmodulated systems, so that this divergence cannot reach large values and efficient tracking can be achieved.

Because of the factor (ii), it is difficult to establish simple precise rules to determine in which systems and in which conditions efficient tracking of steady states can be achieved in a wide domain of modulation frequencies. In particular, it does not seem to be directly determined by the values of the characteristic exponents describing the stability of the steady-state solution, nor by the subcritical or supercritical character of the local bifurcations affecting that solution. Rather, it seems to be determined by qualitative dynamic features of the modulation process—such as factor (ii) above—and symmetry considerations. Factor (ii) is contrary to what would be expected from simplistic approaches, but it occurs at least for the two models considered in this work (and for the model of Ref. [13] pointed out above). It is well known that parameter sweeping or modulation, even when it is slow, can strongly modify the dynamic behavior of a nonlinear system, in a way that can hardly be predicted from simple reasoning. It would be interesting to investigate whether factor (ii) occurs in most nonlinear systems or not, and to what point it can be influenced by the values of the characteristic exponents of the local stable and unstable manifolds of the tracked steady state, in order to ascertain the degree of generality of the tracking effect here described.

ACKNOWLEDGMENTS

Financial support from the Spanish DGICYT (Contract No. PB95-0778-C02) and Generalitat de Catalunya is acknowledged. A.K. also acknowledges financial support from the Comisión Interministerial de Ciencia y Tecnología of the Spanish Goverment, Ref. No. SB96-A00657493.

[1] A. Hübler, R. Georgii, M. Kuckler, W. Stelzl, and E. Lüscher, Helv. Phys. Acta **61**, 897 (1988).

[2] E. Ott, C. Grebogi, and Y. A. Yorke, Phys. Rev. Lett. **64**, 1196 (1990).

[3] See, for instance, *Control and Synchronization of Chaos*, special issue of Chaos **7** (1997).

[4] Z. Gills, C. Iwata, R. Roy, I. Schwartz, and I. Triandaf, Phys. Rev. Lett. **69**, 3169 (1992); I. Schwartz and I. Triandaf, Phys. Rev. A **46**, 7439 (1992); T. Carroll, I. Triandaf, I. Schwartz, and L. Pecora, *ibid.* **46**, 6189 (1992).

[5] I. Schwartz, T. Carr, and I. Triandaf, Chaos **7**, 664 (1997), and references therein.

[6] R. Vilaseca, A. Kul'minskii, and R. Corbalán, Phys. Rev. E **54**, 82 (1996).

[7] R. Dykstra, A. Rayner, D. Y. Tang, and N. R. Heckenberg, Phys. Rev. E **57**, 397 (1998).

[8] A. N. Pisarchik, V. N. Chizhevsky, R. Corbalán, and R. Vilaseca, Phys. Rev. E **55**, 2455 (1998).

[9] C. O. Weiss and R. Vilaseca, *Dynamics of Lasers* (VCH, Weinheim, 1991).

[10] P. Mandel, *Theoretical Problems in Cavity Nonlinear Optics* (Cambridge University Press, Cambridge, 1997).

[11] C. Lepers, J. Legrand, and P. Glorieux, Phys. Rev. A **43**, 2573 (1991).

[12] H. Haken, *Light* (North-Holland, Amsterdam, 1985), Vol. 2.

[13] A. Kul'minskii, R. Vilaseca, and R. Corbalán, J. Opt. Soc. Am. B **16**, 1049 (1999).